

PAPER

Atomic-scale patterning in two-dimensional van der Waals superlattices

To cite this article: Paul Masih Das *et al* 2020 *Nanotechnology* **31** 105302

View the [article online](#) for updates and enhancements.



IOP | ebooks™

Bringing you innovative digital publishing with leading voices to create your essential collection of books in STEM research.

Start exploring the collection - download the first chapter of every title for free.

Atomic-scale patterning in two-dimensional van der Waals superlattices

Paul Masih Das¹ , Jothi Priyanka Thiruraman^{1,2} , Meng-Qiang Zhao¹ ,
Srinivas V Mandyam¹ , A T Charlie Johnson¹  and Marija Drndić¹ 

¹ Department of Physics and Astronomy, University of Pennsylvania, Philadelphia, PA United States of America

² Department of Electrical and Systems Engineering, University of Pennsylvania, Philadelphia, PA United States of America

E-mail: drndic@physics.upenn.edu

Received 13 September 2019, revised 4 November 2019

Accepted for publication 20 November 2019

Published 20 December 2019



CrossMark

Abstract

Two-dimensional (2D) van der Waals superlattices comprised of two stacked monolayer materials have attracted significant interest as platforms for novel optoelectronic and structural behavior. Although studies are focused on superlattice fabrication, less effort has been given to the nanoscale patterning and structural modification of these systems. In this report, we demonstrate the localized layer-by-layer thinning and formation of nanopores/defects in 2D superlattices, such as stacked MoS₂-WS₂ van der Waals heterostructures and chemical vapor deposited bilayer WSe₂, using aberration-corrected scanning transmission electron microscopy (STEM). Controlled electron beam irradiation is used to locally thin superlattices by removing the bottom layer of atoms, followed by defect formation through ablation of the second layer of atoms. The resulting defects exhibit atomically-sharp pore edges with tunable diameters down to 0.6 nm. Structural periodicities and focused STEM irradiation are also utilized to form close-packed nanopore arrays in superlattices with varying twist angles and commensurability. Applying these methods and mechanisms provides a forward approach in the atomic-scale patterning of stacked 2D nanodevices.

Keywords: superlattice, van der Waals heterostructure, bilayers, moire, TEM, quasicrystal, nanopore

(Some figures may appear in colour only in the online journal)

1. Introduction

Vertically stacked layers of two-dimensional (2D) materials with an interlayer twist angle offer a host of exciting electronic, optical, and structural properties. In recent years, these lateral superlattices consisting of two identical (i.e. bilayers) and different (i.e. van der Waals (vdW) heterostructures) stacked 2D materials have demonstrated novel phenomena such as the fractal quantum Hall effect [1], unconventional superconductivity [2], and interlayer excitons [3, 4]. Unlike pure monolayer 2D materials, interlayer twist angle offers an extra degree of freedom in controlling the properties of the stacked systems [5, 6] with increasing efforts focused on producing bilayers and heterostructures with tunable twist angles and stacking orders [4, 7, 8]. Similarly, patterning

structures such as defects, nanoribbons, nanopores, and nanomeshes has been broadly implemented as a method of precisely engineering properties in monolayer 2D materials [9–12] but have received little to no attention in the context of 2D superlattices.

A variety of techniques such as electron beam irradiation/lithography [12, 13], focused ion beam irradiation [14, 15], and block copolymer lithography [10, 16] have been utilized to pattern 2D materials at the atomic scale. Among them, irradiation through sub-nm transmission electron microscopy (TEM) beams allows for lattice reconstructions and atom-by-atom manipulation at unprecedented length scales. For instance, nm-scale holes (i.e. nanopores) drilled in monolayer 2D materials via focused TEM beam exposure have been widely investigated as next-generation avenues for

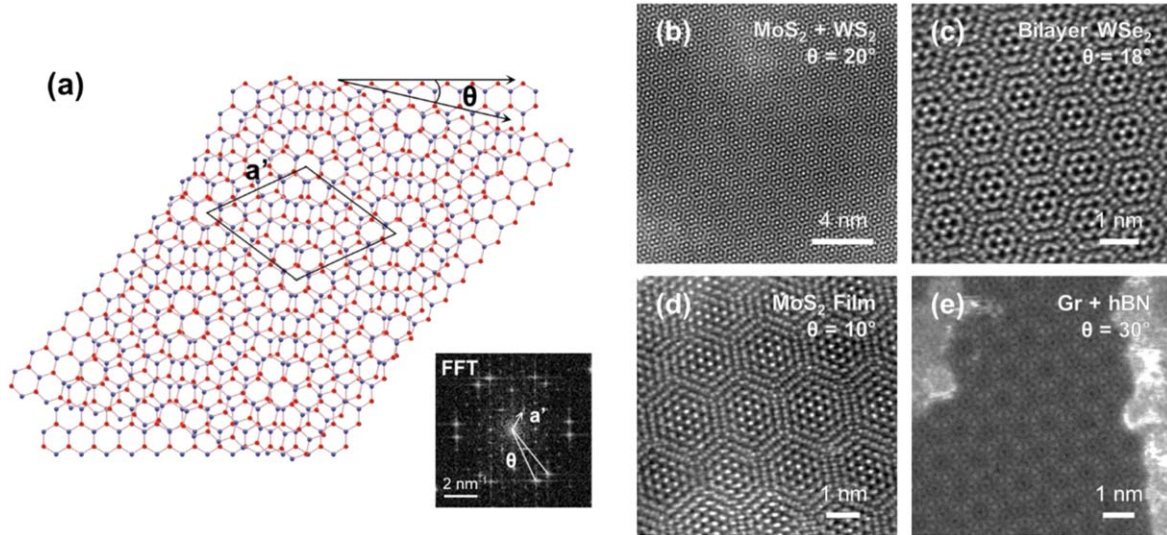


Figure 1. (a) Schematic of moiré pattern formation in a superlattice of two rotationally misaligned monolayer 2D materials. (Inset) Structural parameters θ (twist angle) and a' (moiré lattice parameter) are present in a fast Fourier transform (FFT) of the superlattice. HAADF STEM images taken at an acceleration voltage of 80 kV of a (b) stacked MoS₂-WS₂ heterostructure, (c) CVD-grown bilayer WSe₂ flake, (d) CVD-grown bilayer MoS₂ film, and (e) stacked Gr-hBN heterostructure. The structure in (e) is an incommensurate quasicrystal as opposed to a periodic moiré pattern.

DNA sequencing, molecular detection, and fluid separation [11, 17, 18]. While recent theoretical studies have even suggested that nanopores in bilayer MoS₂ exhibit enhanced biosensing capabilities in comparison to monolayer MoS₂ because of longer pore-protein interaction times [19], experimental characterization of such patterned systems is lacking. In order to fully realize superlattice nanodevices, additional efforts on the nanoscale patterning and characterization of vdW heterostructures and bilayers are required.

In this study, we show the production and atomic-scale characterization of a variety of 2D superlattices including chemical vapor deposition (CVD)-grown bilayers, transferred vdW heterostructures, and quasicrystals. Scanning TEM (STEM) beams are used to pattern these materials through *in situ* layer-by-layer thinning and nanopore/defect formation with sub-nm precision. We also examine the atomic configuration of individual pores and demonstrate the fabrication of nanoporous arrays by employing inherent structural periodicities in the 2D superlattices.

2. Methods

Transition metal dichalcogenide flakes including 1L (monolayer) MoS₂ [20], 1L WS₂ [21], and 2L (bilayer) WSe₂ [22] were grown on Si/SiO₂ substrates through CVD processes described elsewhere. Materials were transferred by spin-coating flakes with PMMA, drying in air for 0.5 h, and overnight etching in room temperature 1M KOH. Flakes were deposited on holey carbon TEM grids, placed in acetone at 80 °C for 4 h, and annealed in Ar/H₂ at 300 °C for 1.5 h. 2L MoS₂ films were grown via Mo foil sulfurization [23] while commercially available 1L graphene (Gr) and 1L hexagonal boron nitride (hBN) on Cu foil were obtained from the Graphene Supermarket. All three were transferred onto TEM

grids using a FeCl₃-based wet etch procedure [23]. MoS₂-WS₂ and Gr-hBN heterostructures were formed by performing the transfer process twice on the same TEM grid.

Selected area electron diffraction (SAED) was performed in a JEOL F200 operating at 200 kV with a 60 cm camera length. Atomic resolution images were obtained with the high-angle annular dark field (HAADF) STEM detector (68–280 mrad) of a spherical aberration-corrected JEOL 200ARM operating at 80 kV. Thinned regions were drilled at room temperature using a probe current $I_{probe} \sim 140$ pA and probe size of ~ 1 Å in STEM spot mode for 10 s (dose $D \sim 1 \times 10^8$ e⁻ Å⁻²). Pores were formed by doubling the exposure time ($D \sim 2 \times 10^8$ e⁻ Å⁻²). We use $I_{probe} \sim 22$ pA and a dwell time of 32 μs/pixel for imaging ($D \sim 4 \times 10^4$ e⁻ Å⁻²). Images were exposed to either an average background subtraction or Gaussian blur filter. Structural analysis was performed using custom-scripted MATLAB and ImageJ software.

3. Results and Discussion

The schematic in figure 1(a) illustrates the principle of moiré pattern formation in a 2D superlattice. When two crystalline monolayers are rotationally misaligned with a twist angle θ ($-30^\circ < \theta < 30^\circ$), the resulting stack forms a moiré pattern with superlattice parameter a' [24, 25]. For a stack of two hexagonal lattice materials, a' is given by:

$$a' = \frac{a}{2 \sin \frac{|\theta|}{2}},$$

where a is the lattice parameter of the monolayer [25].

These long-range structural parameters are delineated in a fast Fourier transform (FFT), which provides a reciprocal

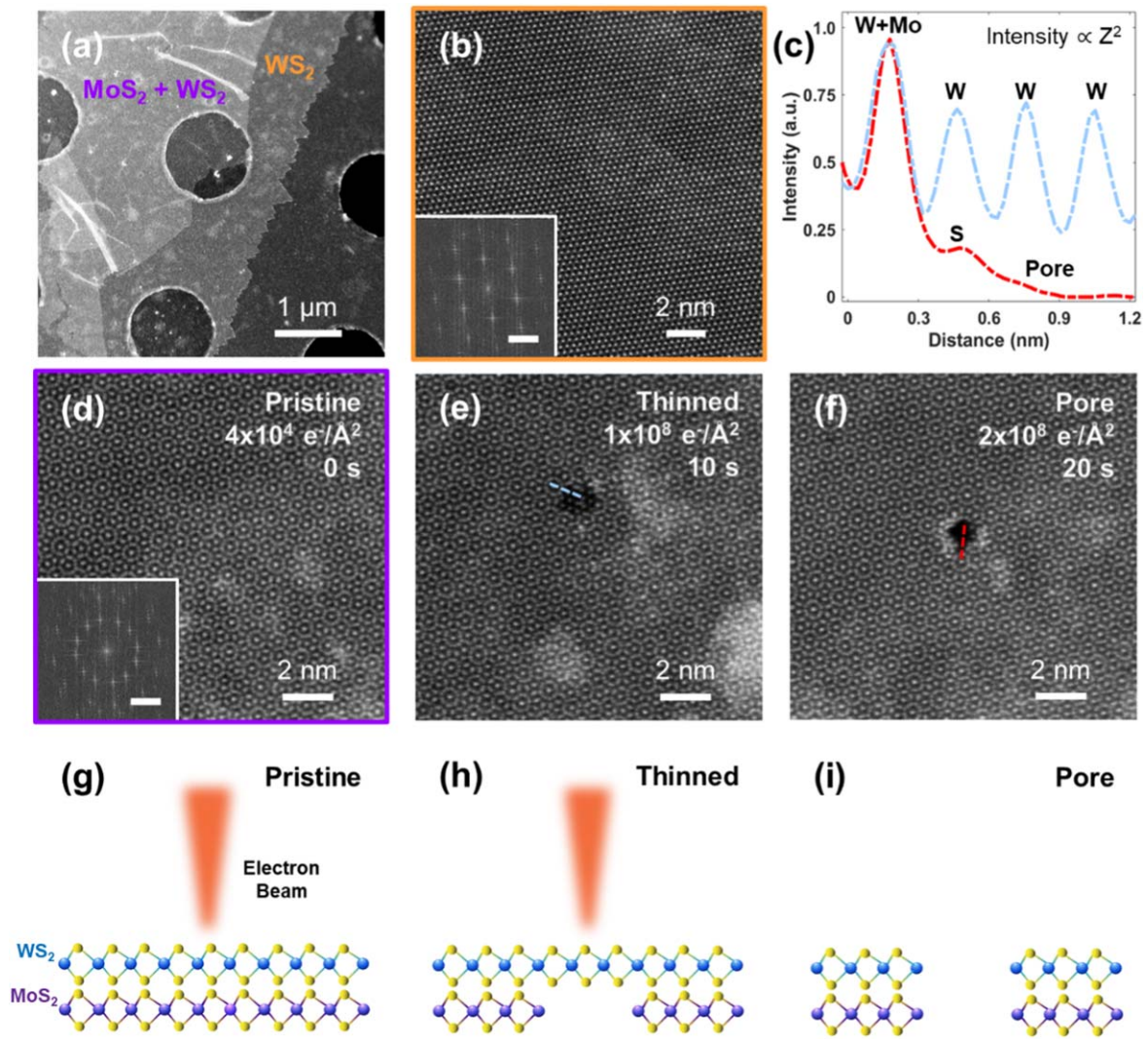


Figure 2. (a) Low magnification STEM image of a MoS₂-WS₂ vdW heterostructure sitting on a holey carbon TEM grid. (b) HAADF STEM image of the overlying WS₂ layer (orange) with (inset) corresponding FFT pattern. (c) Line intensity profiles of the segment shown in (e) and (f), indicating the presence of WS₂ in the thinned region and an intensity drop over the pore, respectively. (d) HAADF STEM image of the MoS₂-WS₂ superlattice region (purple) with (inset) corresponding FFT pattern displaying $\theta \sim 25^\circ$. Exposure to a focused STEM beam results in (e) the formation of a thinned region ($d \sim 1.0$ nm) after 10 s and (f) eventually a nanopore ($d \sim 1.0$ nm) after a total of 20 s. (g) Schematic demonstrating how focused electron beam irradiation of 2D bilayers and vdW heterostructures causes ablation to occur (h) first in the bottom monolayer and (i) subsequently the top monolayer, resulting in a pore.

space representation of a superlattice. The pattern in the inset of figure 1(a) is an FFT of an atomic resolution STEM image and indicates a stack of two hexagonal lattice monolayers with $\theta \sim 14^\circ$, resulting in a superlattice with $a' \sim 0.79$ nm.

2D superlattices with precisely engineered twist angles can be produced through a variety of different techniques. The most widely applied method consists of physically stacking two monolayer materials. Figure 1(b) shows an 80 kV HAADF STEM image of a vdW heterostructure with two CVD-grown monolayers (1L MoS₂ and 1L WS₂) that have been randomly stacked ($\theta \sim 20^\circ$) with a wet transfer technique (see Methods). We note that advances in dry transfer techniques further allow for tunable twist angles with down to $\sim 0.1^\circ$ precision [24, 26].

Superlattices can also be fabricated through CVD growth of bilayer 2D materials. Figures 1(c) and (d) exhibit bilayer

WSe₂ flakes ($\theta \sim 18^\circ$) and bilayer MoS₂ films ($\theta \sim 10^\circ$), respectively, that have been produced with CVD [22, 23]. Other studies have been aimed at the growth of vdW heterostructures with novel interlayer optoelectronic properties [8, 27, 28]. However, CVD growth currently offers poor control over twist angle compared to mechanical stacking such that further efforts are needed to engineer bilayer and heterostructure systems with particular geometries and materials. Beyond regular moiré patterns, superlattices also enable investigations of incommensurate structures with no long-range periodicities [29, 30], such as the 30°-twisted quasi-crystal of stacked graphene (Gr) and hexagonal boron nitride (hBN) shown in figure 1(d).

In addition to physical characterization, focused STEM beams enable the fabrication of nanopores and sub-nm vacancies in ultrathin materials through atomic-scale ablation.

Nanopores have previously been reported in monolayer 2D materials such as graphene [31], hBN [32], MoS₂ [17], WS₂ [11], and various transition metal carbides (MXenes) [33] using this technique. Here, we extend these methods to demonstrate the fabrication of nanopores in stacked vdW heterostructures (figures 2, 3) and bilayers (figure 4) using STEM, and investigate the resulting structural properties. Figure 2(a) is a low magnification STEM image of a MoS₂-WS₂ heterostructure sitting on a holey carbon TEM grid. Atomic resolution imaging of the capping monolayer reveals a lattice that is consistent with previous reports of monolayer WS₂ (orange, figure 2(b)) [11, 34, 35]. The corresponding FFT pattern similarly indicates a lattice spacing (2.71 Å) that is in excellent agreement with the (100) lattice parameter of 2H-phase monolayer WS₂ [36]. STEM imaging of the superlattice region shows a quasicrystal structure with twist angle $\theta \sim 25^\circ$ (purple, figure 2(d)).

In monolayer 2D materials, STEM-based drilling results in nanopore formation due to collisions between lattice atoms and incident electrons [37]. In two layers, we observe that focusing a STEM beam (i.e. spot mode) with probe current $I_{probe} \sim 140$ pA on the superlattice for 10 s (dose $D \sim 1 \times 10^8$ e⁻ Å⁻²) first creates a thinned region with diameter $d \sim 1.0$ nm as opposed to a nanopore (figure 2(e)). As demonstrated in figures 2(c) and (e), an intensity profile (outlined in blue) across the boundary shows that the crystalline nature of the thinned region is retained. Furthermore, the dependence of HAADF image intensity on atomic number (Z) by $\sim Z^2$ enables determination of the thinned region composition [14, 38]. As demonstrated by others, here we normalize the maximum HAADF intensity in STEM images to a value of 1.0 [39]. For the MoS₂-WS₂ heterostructure in figure 2, maximum HAADF intensity occurs at sites contained overlapping Mo and W atoms. Compared to the intensity of 0.97–1.0 for these superlattice sites (figure 2(c), ‘W + Mo’), sites in the thinned region have an intensity of ~ 0.69 (figure 2(c), ‘W’). This is indicative of W atoms, thus showing that the thinned region is comprised of WS₂ and that the MoS₂ layer is removed before the WS₂ layer. Here, the use of a vdW heterostructure enables the nanostructural analysis of individual layers during the thinning and pore formation processes, which would otherwise not be possible in vdW bilayers with identical 2D monolayers (for example, see figure 4). These energetics are demonstrated schematically in figures 2(g)–(i) and suggests that during the first 10 s of exposure, the MoS₂ monolayer prevents electron beam knock-on damage in the WS₂ monolayer. This observation explains the success of previous approaches in preventing 2D material radiation damage by graphene encapsulation [37, 40] as well as the STEM thinning of ultrathin (i.e. few nm) silicon nitride (SiN_x) membranes at 200 kV [41]. Further exposure of the thinned region to the focused STEM beam for another 10 s ($D \sim 2 \times 10^8$ e⁻ Å⁻²) causes displacement of the W and S atoms [42, 43], resulting in the formation of a pore in the MoS₂-WS₂ heterostructure (figure 2(f)). As shown in figure 2(c) (red), the profile shows a drastic reduction in intensity due to residual chalcogen atoms at the pore edge as well as a complete absence of intensity in the pore interior,

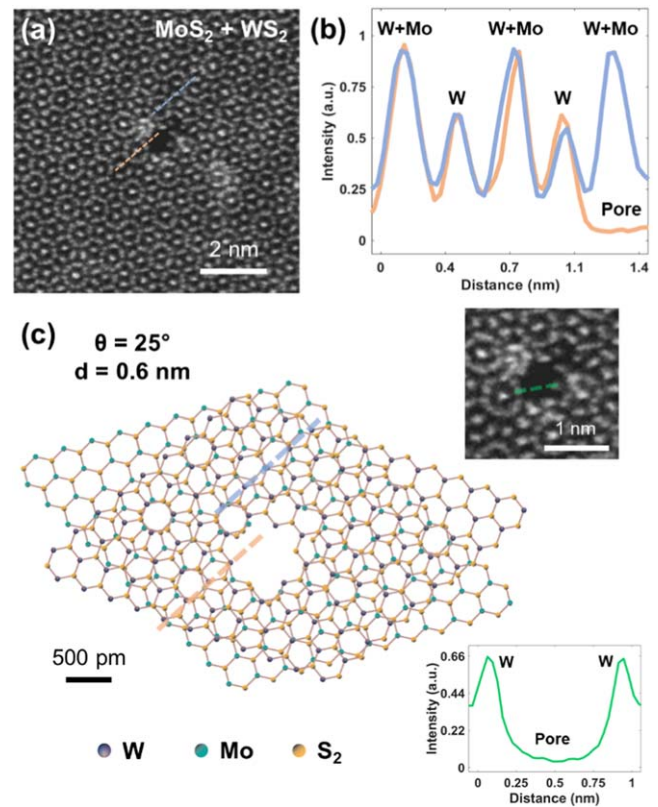


Figure 3. (a) HAADF STEM image of a single nanopore/defect with $d \sim 0.6$ nm in a MoS₂-WS₂ vdW heterostructure ($\theta \sim 25^\circ$) drilled with focused electron beam irradiation. (b) Line intensity profiles of the segments shown in (a), showing (orange) a drop in intensity at the nanopore in comparison to (blue) a pristine region of the quasicrystalline superlattice. (c) Atomic model and (top inset) high magnification STEM image of the pore shown in (a) with corresponding intensity profile segments. (Bottom inset) Line intensity profile of the segment (green) shown in the top inset, showing the edge of the pore.

indicating ablation of both heterostructure layers. Due to the fact that the pore has the same diameter as the thinned region ($d \sim 1.0$ nm), STEM thinning of 2D superlattices offers a way of avoiding the unintended formation of multiple pores/defects (e.g. as in monolayer 2D materials) [37, 44–46] or as a method of localizing pore formation during dielectric breakdown processes [47].

Utilizing sub-nm aberration-corrected electron beams also allows for pore fabrication in 2D materials with tunable sizes down to a few atoms. A MoS₂-WS₂ superlattice region is first thinned for 10 s as described above. Further exposing the thinned region to a focused STEM beam for half the time (5 s, $D \sim 5 \times 10^7$ e⁻ Å⁻²) compared to figure 2(f) (10 s, $D \sim 1 \times 10^8$ e⁻ Å⁻²) results in a smaller pore ($d \sim 0.6$ nm). A HAADF STEM image reveals that this is due to incomplete ablation of the thinned region, resulting in a patch of intact monolayer WS₂ at the top right edge of the pore (figure 3(a)), further confirming the aforementioned thinning process (see figure 2). The atomically-sharp edges of the pore are clearly evident from the line intensity profiles of the pore and pore edge in figure 3(c) (green) and figure 3(b) (orange), respectively. Similarly, the STEM image in figure 3(a) demonstrates

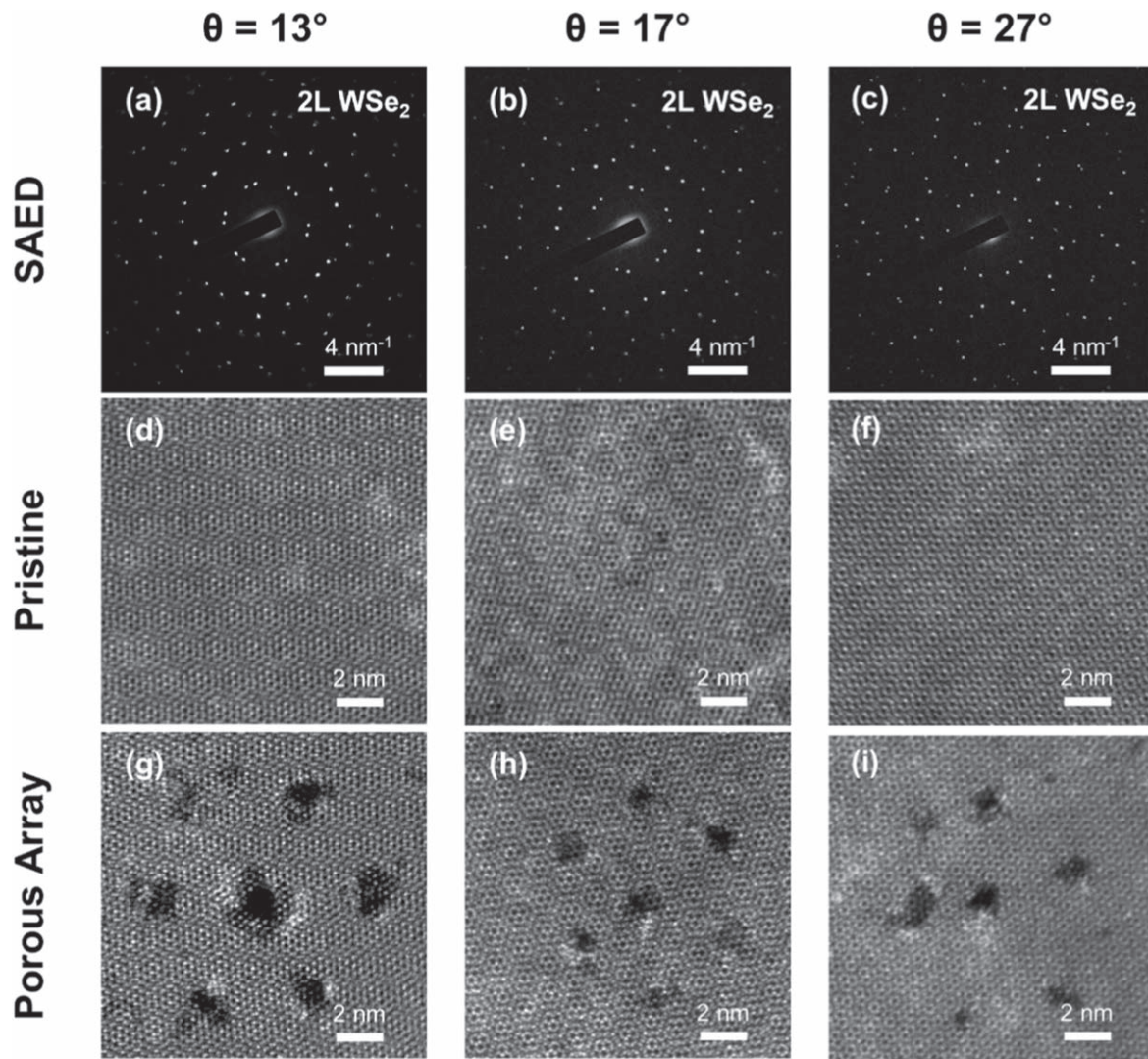


Figure 4. (a)–(c) SAED patterns and (d)–(f) HAADF STEM lattice images of CVD-grown bilayer WSe₂ flakes with (a,d) $\theta \sim 13^\circ$, (b), (e) $\theta \sim 17^\circ$, and (c), (f) $\theta \sim 27^\circ$. The moiré pattern provides a close-packed, hexagonal lattice template for STEM-based nanopore array drilling. (g–i) STEM images of nanopore arrays with inter-pore distance $L_D \sim 4\text{--}5$ nm drilled in flakes at different twist angles. L_D roughly corresponds to $\sim 2a'$, $3a'$, and $5a'$ (a' = moiré lattice parameter) for bilayer WSe₂ with (g) $\theta \sim 13^\circ$, (h) $\theta \sim 17^\circ$, and (i) $\theta \sim 27^\circ$.

that moiré superlattice of the region surrounding the pore remains unperturbed. This demonstrates that pore formation process outlined here preserves the crystallinity of the superlattice, unlike previous reports of monolayer 2D materials in which strong electron beams cause amorphization of the pore edge [17, 44]. The atomic structure of the pore with $d \sim 1.0$ nm in figure 2(f) can also be discerned despite the presence of ejected atoms. Figure 3(c) is an atomic model of the superlattice pore with W, Mo, and S₂ lattice sites represented in purple, green, and yellow, respectively. The $d \sim 0.6$ nm pore constitutes a total of 3 W and 6 S atoms removed from the top WS₂ layer and 6 Mo and 10 S atoms missing from the underlying MoS₂ layer (error of ± 1 atom due to electron beam aberrations and the low HAADF contrast of sulfur).

In vdW heterostructures and bilayers, it is possible to tailor optical and electronic properties by varying θ , the interlayer twist angle. Figures 4(a)–(c) exhibit SAED patterns

from CVD-grown bilayer WSe₂ flakes with twist angles of 13° , 17° , and 27° , respectively, on a holey carbon TEM grid. HAADF STEM images show periodic moiré superlattices for each value of θ (figures 4(d)–(f)). Advances in STEM software-hardware interfaces now enable *in situ* focused electron beam patterning with sub-nm precision and are widely utilized to induce defect formation, lattice reconstructions, and low-dimensional nanostructures in 2D materials [46, 48, 49]. By controllably exposing a pristine bilayer region to the focused STEM probe using the conditions outlined in figure 2 (20 s exposure per pore; $D \sim 2 \times 10^8$ e⁻ Å⁻²), arrays of nanopores in a hexagonal lattice pattern are produced. The resulting porous array has a close-packed structure, which ensures a uniform spacing between neighbouring pores as well as a more efficient packing fraction compared to conventional square arrays [13, 50]. Across different twist angles, a fixed inter-pore distance (L_D) of $\sim 4\text{--}5$ nm was maintained. While identical exposure conditions are used across samples

with different θ , we note that pores occasionally do not drill completely through both layers or possess different diameters due to stage drift within the electron microscope and local variations in polymer contamination (figures 4(g)–(i)). The porous array fabrication process can be further improved with cleaner samples through polymer-free transfer [51] and/or *in situ* annealing [52]. As shown in figure 4(g), the L_D range of ~ 4 – 5 nm is equivalent to approximately two moiré lattice parameters ($L_D \sim 2a'$) in bilayer WSe₂ with $\theta \sim 13^\circ$, meaning that the center of each pore is spaced roughly two superlattice unit cells apart. Similarly, $L_D \sim 3a'$ and $L_D \sim 5a'$ holds for larger twist angles of $\theta \sim 17^\circ$ (figure 4(h)) and $\theta \sim 27^\circ$ (figure 4(i)), respectively. The hexagonal periodicity of moiré superlattices in twisted bilayers and vdW heterostructures therefore provides an intrinsic template for patterning nanoporous arrays and other low-dimensional structures at the atomic scale.

4. Conclusion

Through the use of controlled electron beam irradiation, we have illustrated the atomic-scale thinning, ablation, and patterning of 2D material superlattices. STEM imaging was used to characterize the commensurability, interlayer twist angle, and moiré lattice parameter of stacked heterostructures of Gr, hBN, MoS₂, and WS₂ fabricated through a wet transfer process as well as CVD-grown bilayer MoS₂ and WSe₂. We studied both periodic moiré and quasicrystalline superlattices with different twist angles from $\theta \sim 10$ – 30° . Under focused electron beam exposure, the bottom layer of superlattice is removed, resulting in the formation of nanoscale thinned regions. By variably focusing a STEM beam on these thinned regions under different exposure times, nanopores/defects with tunable sizes down to $d \sim 0.6$ nm (comparable to 2D lattice spacings) can also be created. We utilized the mass-contrast behavior of HAADF imaging to investigate the structural characteristics of the resulting pores and show that thinned regions and pore edges retain their crystallinity after electron beam exposure. Electron diffraction and STEM imaging provide insights into the nanoscale periodicities of bilayers with varying structural parameters. These periodicities were employed to pattern close-packed arrays of pores while the correlation between inter-pore distance, bilayer twist angle, and moiré lattice parameter was examined. With increasing interest in multilayer 2D architectures, these results motivate further studies on the structural characterization and modification of vdW superlattices.

Acknowledgments

We thank Dr Eric Stach and Dr Douglas Yates of the University of Pennsylvania, Dr Robert Keyse of Lehigh University, and Hashiguchi Hiroki of JEOL Ltd for their assistance with STEM imaging. This research was primarily supported by the NSF through the University of Pennsylvania Materials Research Science and Engineering Center (MRSEC) DMR-1720530

as well as NSF Grants EFRI 2-DARE 1542707, EAGER 1838456, and DMR 1905045 ('In Situ TEM and Ex Situ Studies of Two-Dimensional Nanostructured Devices'). M.Q.Z and A.T.C.J. acknowledge support from NSF Grants EFRI 2-DARE 1542879 and EAGER 1838412. This work was performed in part at the University of Pennsylvania's Singh Center for Nanotechnology, an NNCI member supported by NSF Grant ECCS-1542153. J P T acknowledges fellowship support from the Vagelos Institute of Energy Science and Technology (VIEST).

ORCID iDs

Paul Masih Das  <https://orcid.org/0000-0003-2644-2280>

Jothi Priyanka Thiruraman  <https://orcid.org/0000-0001-5089-491X>

Meng-Qiang Zhao  <https://orcid.org/0000-0002-0547-314>

Srinivas V Mandyam  <https://orcid.org/0000-0003-1927-7678>

A T Charlie Johnson  <https://orcid.org/0000-0002-5402-1224>

Marija Drndić  <https://orcid.org/0000-0002-8104-2231>

References

- [1] Wang L, Gao Y, Wen B, Han Z, Taniguchi T, Watanabe K, Koshino M, Hone J and Dean C R 2015 *Science* **350** 1231
- [2] Cao Y, Fatemi V, Fang S, Watanabe K, Taniguchi T, Kaxiras E and Jarillo-Herrero P 2018 *Nature* **556** 43
- [3] Tran K *et al* 2019 *Nature* **567** 71
- [4] Shih C K, Li L J, Ren X, Zhang C, Jin C, Chou M Y, Chuu C P and Li M Y 2017 *Sci. Adv.* **3** e1601459
- [5] Jin C *et al* 2019 *Nature* **567** 76
- [6] Bistrizter R and MacDonald A H 2011 *Proc. Natl Acad. Sci.* **108** 12233
- [7] Zheng S, Sun L, Zhou X, Liu F, Liu Z, Shen Z and Fan H J 2015 *Adv. Opt. Mater.* **3** 1600
- [8] Zhang Z *et al* 2017 *ACS Nano* **11** 4328
- [9] Liu X *et al* 2013 *Nat. Commun.* **4** 1776
- [10] Bai J, Zhong X, Jiang S, Huang Y and Duan X 2010 *Nat. Nanotechnol.* **5** 190
- [11] Danda G *et al* 2017 *ACS Nano* **11** 1937
- [12] Cupo A, Masih Das P, Chien C C., Danda G, Khariche N, Tristant D, Drndić M and Meunier V 2017 *ACS Nano* **11** 7494
- [13] Verschueren D V, Yang W and Dekker C 2018 *Nanotechnology* **29** 145302
- [14] Thiruraman J P *et al* 2018 *Nano Lett.* **18** 1651
- [15] Fox D S *et al* 2015 *Nano Lett.* **15** 5307
- [16] Kim M, Safron N S, Han E, Arnold M S and Gopalan P 2010 *Nano Lett.* **10** 1125
- [17] Liu K, Feng J, Kis A and Radenovic A 2014 *ACS Nano* **8** 2504
- [18] Rollings R C, Kuan A T and Golovchenko J A 2016 *Nat. Commun.* **7** 11408
- [19] Nicolai A, Barrios Pérez M D, Delarue P, Meunier V, Drndić M and Senet P 2019 *J. Phys. Chem. B* **123** 2342
- [20] Naylor C H, Kybert N J, Schneier C, Xi J, Romero G, Saven J G, Liu R and Charlie Johnson A T 2016 *ACS Nano* **10** 6173

- [21] Danda G, Masih Das P and Drndic M 2018 *2D Mater.* **5** 035011
- [22] Mandyam S, Zhao M Q, Masih Das P, Zhang Q, Price C, Drndic M, Shenoy V and Charlie Johnson A T 2019 *ACS Nano* **13** 10490
- [23] Masih Das P, Thiruraman J P, Chou Y C, Danda G and Drndic M 2019 *Nano Lett.* **19** 392
- [24] Woods C R *et al* 2014 *Nat. Phys.* **10** 451
- [25] Liao Y, Cao W, Connell J W, Chen Z and Lin Y 2016 *Sci. Rep.* **6** 26084
- [26] Ribeiro-Palau R, Zhang C, Watanabe K, Taniguchi T, Hone J and Dean C R 2018 *Science* **361** 690
- [27] Gong Y *et al* 2014 *Nat. Mater.* **13** 1135
- [28] Zhou X *et al* 2017 *2D Mater.* **4** 025048
- [29] Yao W *et al* 2018 *Proc. Natl Acad. Sci.* **115** 6928
- [30] Moon P, Koshino M and Son Y W 2019 *Phys. Rev. B* **99** 165430
- [31] Merchant C A *et al* 2010 *Nano Lett.* **10** 2915
- [32] Liu S *et al* 2013 *Adv. Mater.* **25** 4549
- [33] Mojtabavi M, Vahidmohammadi A, Liang W, Beidaghi M and Wanunu M 2019 *ACS Nano* **13** 3042
- [34] Ryu G H, France-Lanord A, Wen Y, Zhou S, Grossman J C and Warner J H 2018 *ACS Nano* **12** 11638
- [35] Thiruraman J P, Masih Das M and Drndic M 2019 *Adv. Funct. Mater.* **1** 1904668
- [36] Mao X, Xu Y, Xue Q, Wang W and Gao D 2013 *Nanoscale Res. Lett.* **8** 430
- [37] Algara-Siller G, Kurasch S, Sedighi M, Lehtinen O and Kaiser U 2013 *Appl. Phys. Lett.* **103** 203107
- [38] Krivanek O L *et al* 2010 *Nature* **464** 571
- [39] Bangert U, Stewart A, O'Connell E, Courtney E, Ramasse Q, Kepaptsoglou D, Hofsäss H, Amani J, Tu J S and Kardynal B 2017 *Ultramicroscopy* **176** 31
- [40] Zan R, Ramasse Q M, Jalil R, Georgiou T, Bangert U and Novoselov K S 2013 *ACS Nano* **7** 10167
- [41] Rodríguez-Manzo J A, Puster M, Nicolai A, Meunier V and Drndić M 2015 *ACS Nano* **9** 6555
- [42] Yoshimura A, Lamparski M, Kharche N and Meunier V 2018 *Nanoscale* **10** 2388
- [43] Komsa H P, Kotakoski J, Kurasch S, Lehtinen O, Kaiser U and Krasheninnikov A V 2012 *Phys. Rev. Lett.* **109** 035503
- [44] Song B, Schneider G F, Xu Q, Pandraud G, Dekker C and Zandbergen H 2011 *Nano Lett.* **11** 2247
- [45] Ryu G H *et al* 2015 *Nanoscale* **7** 10600
- [46] Parkin W M, Balan A, Liang L, Masih Das P, Lamparski M, Naylor C H, Rodríguez-Manzo J A, Charlie Johnson A T, Meunier V and Drndić M 2016 *ACS Nano* **10** 4134
- [47] Kuan A T, Lu B, Xie P, Szalay T and Golovchenko J A 2015 *Appl. Phys. Lett.* **106** 203109
- [48] Masih Das P *et al* 2016 *ACS Nano* **10** 5687
- [49] Bayer B C, Kaindl R, Monazam M R A, Susi T, Kotakoski J, Gupta T, Eder D, Waldhauser W and Meyer J C 2018 *ACS Nano* **12** 8758
- [50] Gilboa T, Zvuloni E, Zrehen A, Squires A H and Meller A 2019 *Adv. Funct. Mater.* **1** 1900642
- [51] Castellanos-Gomez A, Buscema M, Molenaar R, Singh V, Janssen L, van der Zant H S J and Steele G A 2014 *2D Mater.* **1** 011002
- [52] Tripathi M, Mittelberger A, Mustonen K, Mangler C, Kotakoski J, Meyer J C and Susi T 2017 *Phys. Status Solidi* **11** 1700124